AJA

Research Article

Auditory Detection Thresholds and Cochlear Resistivity Differ Between Pediatric Cochlear Implant Listeners With Enlarged Vestibular Aqueduct and Those With Connexin-26 Mutations

Kelly N. Jahn,[a,b] Molly D. Bergan,[c] and Julie G. Arenberg[a,b]

Purpose: The goal of this study was to evaluate differences in the electrode–neuron interface as a function of hearing loss etiology in pediatric cochlear implant (CI) listeners with enlarged vestibular aqueduct (EVA) syndrome and in those with autosomal recessive connexin-26 mutations (DFNB1).
Method: Fifteen implanted ears (9 participants, 5 ears with EVA, 10 ears with DFNB1) were assessed. Single-channel auditory detection thresholds were measured using broad and spatially focused electrode configurations (steered quadrupolar; focusing coefficients = 0 and 0.9). Cochlear resistivity estimates were obtained via electrode impedances and electrical field imaging. Between-group differences were evaluated using linear mixed-effects models.
Results: Children with EVA had significantly higher auditory detection thresholds than children with DFNB1, irrespective of electrode configuration. Between-group differences in thresholds were more pronounced on apical electrodes than on basal electrodes. In the apex, electrode impedances and electrical field imaging values were higher for children with EVA than for those with DFNB1.
Conclusions: The electrode–neuron interface differs between pediatric CI listeners with DFNB1 and those with EVA. It is possible that optimal clinical interventions may depend, in part, on hearing loss etiology. Future investigations with large samples should investigate individualized CI programming strategies for listeners with EVA and DFNB1.

Children with cochlear implants (CIs) exhibit highly variable speech and language outcomes (e.g., Huber & Kipman, 2012; Niparko et al., 2010; Sarant, Harris, & Bennet, 2015). One factor that might contribute to this variability is the quality of the electrode–neuron interface (ENI) or the fidelity of information transfer between each CI channel and the auditory nerve. The efficacy with which CI electrodes interface with their target spiral ganglion neurons (SGNs) is believed to be influenced by several factors, including the degree of intracochlear bone and fibrous tissue growth (Jahn & Arenberg, 2019a; Spelman, Clopton, & Pfingst, 1982), electrode position relative to the target SGNs (DeVries, Scheperle, & Bierer, 2016; Long et al., 2014), and the density and integrity of the remaining SGNs (Goldwyn, Bierer, & Bierer, 2010; Jahn & Arenberg, 2019b). While factors that influence the ENI have been studied extensively in adult CI listeners (e.g., Bierer & Faulkner, 2010; DeVries et al., 2016; Jahn & Arenberg, 2019a; Long et al., 2014; Nelson, Donaldson, & Kreft, 2008; Padilla & Landsberger, 2016; Zhu, Tang, Zeng, Guan, & Ye, 2012), little is understood about the ENI in children.

Available evidence suggests that common causes of pediatric deafness can systematically influence the quality of the ENI. For instance, cochlear malformations likely impact the placement of the electrodes relative to target SGNs, which influences the level of current necessary to elicit auditory percepts (Coelho & Roland, 2012; Papsin, 2005). Children with auditory nerve deficiency have

[a]Department of Otolaryngology–Head and Neck Surgery, Harvard Medical School, Boston, MA
[b]Eaton-Peabody Laboratories, Massachusetts Eye and Ear Infirmary, Boston
[c]Department of Speech and Hearing Sciences, University of Washington, Seattle
Correspondence to Kelly N. Jahn: kelly_jahn@meei.harvard.edu

Editor-in-Chief: Sumitrajit Dhar
Editor: Monita Chatterjee
Received April 22, 2019
Revision received June 11, 2019
Accepted October 13, 2019
https://doi.org/10.1044/2019_AJA-19-00054

Disclosure: *The authors have declared that no competing interests existed at the time of publication.*

reduced evoked potential responses (He et al., 2018) and require higher stimulus current levels to achieve threshold and maximum comfortable levels than children with other etiologies (Incerti et al., 2018). Moreover, increased cochlear resistivity in postmeningitic CI listeners leads to relatively high current level requirements (Durisin et al., 2015; Eshraghi, Telischi, Hodges, Odabasi, & Balkany, 2004). Each of these findings suggests that different disease processes associated with severe-to-profound hearing impairment in children likely result in distinct profiles of electrode position relative to the SGNs, SGN integrity, and/or intracochlear bone and tissue growth. In turn, etiology-related differences in the ENI influence programming parameters for individual children.

However, existing research evaluating the ENI and programming characteristics in pediatric CI listeners is sparse and focuses primarily on comparing broad etiological groups. Often, children with "normal cochlear anatomy" are compared to those with varying degrees of cochlear malformations or ossification, which can encompass a variety of underlying impairments (Coelho & Roland, 2012; Eisenman, Ashbaugh, Zwolan, Arts, & Telian, 2001; Incerti et al., 2018; Papsin, 2005). In particular, there is a dearth of evidence that independently evaluates the ENI for two of the most common etiologies associated with severe-to-profound sensorineural hearing loss in children with CIs: enlarged vestibular aqueduct (EVA) syndrome and connexin-26 (Cx26) genetic mutations. The goal of this study was to characterize single-channel auditory detection thresholds and cochlear resistivity in a small sample of pediatric CI listeners with EVA and with Cx26-based deafness.

Five percent to 15% of children with sensorineural hearing loss have EVA, making it the most common morphogenetic cause of hearing impairment in children (Berrettini et al., 2005; Davidson et al., 1999; National Institute on Deafness and Other Communication Disorders [NIDCD], 2017). EVA syndrome is characterized by the presence of an abnormally large vestibular aqueduct (anteroposterior diameter $\geq$ 1.5 mm) and frequently co-occurs with mild structural abnormalities of the cochlea, modiolus, vestibule, and semicircular canals (Berrettini et al., 2005; Davidson et al., 1999; Ito et al., 2014; Vijayasekaran et al., 2007). Notably, most individuals with EVA have modiolar deficiencies, even if cochlear anatomy is normal (Davidson et al., 1999; Lemmerling, Mancuso, Antonelli, & Kubilis, 1997). Differences in cochlear dimensions can alter electrode placement relative to the auditory nerve, and modiolar deficiency may impact the integrity or the total number of functional SGNs. Currently, the influence of abnormal cochlear and modiolar morphology on the quality of the ENI in children with EVA is poorly understood.

Approximately 50% of childhood nonsyndromic sensorineural hearing loss is caused by mutations in the GJB2/DFNB1 gene, which encodes the Cx26 gap junction protein (Cohn et al., 1999; Dahl et al., 2001). In contrast to EVA, DFNB1 is not generally associated with vestibular or cochlear structural abnormalities (Cohn et al., 1999; Del Castillo & Del Castillo, 2017; Kemperman, Hoefsloot, & Cremers, 2002). Little is known about the status of the auditory nerve in patients with DFNB1 mutations. However, Jun et al. (2000) demonstrated that a temporal bone of one adult CI listener with Cx26-related deafness had a normal population of SGNs and no peripheral neural degeneration. Overall, available evidence suggests that children with Cx26 mutations may have less variation in cochlear anatomy and, possibly, SGN integrity, relative to children with EVA.

We predicted that the relatively typical morphological development of the inner ear and modiolus in children with DFNB1 would result in lower single-channel behavioral thresholds relative to children with EVA. We also predicted that intracochlear resistance would differ between groups, as assessed via electrode impedances and electrical field imaging (EFI). The results of this investigation will provide insight into whether the ENI is related to hearing loss etiology in children with CIs and facilitate further investigation into optimal programming parameters for listeners with common causes of childhood deafness.

Method

Participants

Participant demographic information is provided in Table 1. Nine children (seven boys, two girls) aged 8–17 years (M = 13.62 years, SD = 2.33 years) who were implanted with Advanced Bionics HiRes90K devices participated. Clinical notes indicated full electrode array insertions for each ear in this study. Duration of deafness was defined as the length of time, in years, between diagnosis of severe-to-profound sensorineural hearing loss (audiometric thresholds of 70 dB HL or greater at octave frequencies between 250 and 8000 Hz) and CI activation. Six children were bilaterally implanted, and the remainder were unilaterally implanted. Each ear was tested separately, yielding a total sample size of 15 ears. Four children (five ears) had confirmed diagnoses of EVA, and five children (10 ears) had confirmed diagnoses of DFNB1. Subjects P11 and P12 are fraternal twins. No other subjects are related to one another. Each child provided informed written assent, and their parents or legal guardians provided informed written consent. All procedures were approved by the University of Washington Human Subjects Division.

All subjects were native American English speakers and primarily used spoken language to communicate. To provide a clinically relevant indication of auditory outcomes for each listener, speech perception scores, measured using a closed-set medial vowel identification task, are presented in Table 1. Vowel identification was assessed for each ear in the laboratory using the child's everyday listening strategy. Unilaterally implanted listeners wore an

Table 1. Demographic information for all ears tested.

ID	Age (years)	First implanted ear: Age implanted (years)	First implanted ear: Duration of deafness (years)	First implanted ear: Vowel score (%)	Second implanted ear: Age implanted (years)	Second implanted ear: Duration of deafness (years)	Second implanted ear: Vowel score (%)
Enlarged vestibular aqueduct							
P02	11.8	1.1	1.1	87	3.1	3.1	100
P08	15.3	2.9	0.5	68.5	—	—	—
P13	11.7	9.2	6.4	71	—	—	—
P15	8.5	7.9	4.9	66.5	—	—	—
M	11.8	5.3	3.2	73.5	—	—	—
(*SD*)	(2.8)	(3.9)	(2.9)	(9.3)			
Connexin-26 mutation (DFNB1)							
P05	17.8	4.1	4.1	96.5	13.9	10.9	86.5
P10	13.4	1.1	1.1	93	5.1	5.1	100
P11	13.3	1.4	1.2	52	10.2	10.0	22
P12	13.3	1.7	1.4	66.7	10.2	10.0	13.5
P16	14.6	1.0	1.0	90	4.5	4.5	95
M	14.5	1.9	1.8	80.0	8.8	8.1	63.4
(*SD*)	(1.9)	(1.3)	(1.3)	(19.4)	(3.9)	(3.0)	(42.1)

Note. Dashes signify that the child was unilaterally implanted.

earplug in the contralateral ear during testing. Stimuli were presented from 0° azimuth at a calibrated level of 60 dB A. The reader is referred to the work of DiNino and Arenberg (2018) for a detailed description of the vowel stimuli and the testing procedure used with children in our laboratory.

Electrical Stimuli

All electrical stimuli were presented directly to the internal device and controlled using the Bionic Ear Data Collection System Version 1.18.315 (Advanced Bionics) and custom MATLAB scripts (MathWorks, Inc.). Stimuli were verified using a reference implant and a digital storage oscilloscope.

Single-Channel Auditory Detection Threshold Measures

Single-channel behavioral auditory detection thresholds were measured in response to both monopolar and focused electrode configurations using a modified sweep procedure that is based on Békésy tracking principles (Bierer, Bierer, Kreft, & Oxenham, 2015; Sek, Alcántara, Moore, Kluk, & Wicher, 2005). The sweep procedure implements current steering to virtually sweep the stimuli across the electrode array, as described below. Current steering divides the electrical current between two adjacent electrodes and varies the proportion of current directed through each electrode. The sweep procedure yields similar absolute threshold estimates to those obtained using traditional adaptive forced-choice procedures; however, thresholds can be obtained across the electrode array up to four times faster with the sweep procedure than with adaptive forced-choice methods (Bierer et al., 2015). This makes the sweep procedure preferable for assessing single-channel behavioral thresholds in children.

For both monopolar and focused electrode configurations, stimuli were biphasic, cathodic-leading pulse trains (102 μs/phase, 0-μs interphase gap, 200.4-ms duration, 997.9 pps) presented using steered quadrupolar (sQP) stimulation. In sQP stimulation, a channel is composed of four intracochlear electrodes, wherein the two middle electrodes are active, and current is returned through two outer electrodes. The current focusing coefficient, sigma (σ), alters the degree of current focusing by specifying the fraction of current delivered through the intracochlear return electrodes, with the remainder flowing through an extracochlear ground. Sigma can range from 0 to 1, such that $\sigma = 0$ represents monopolar stimulation, wherein all of the return current is delivered through the extracochlear ground electrode. A sigma value of 1 represents the highest possible degree of current focusing, where all return current is delivered through the intracochlear return electrodes (i.e., 50% of the return current is delivered through each of the two return electrodes). In this study, thresholds were measured in response to monopolar stimulation ($\sigma = 0$) and in response to a highly focused electrode configuration with $\sigma = 0.9$.

For some CI listeners, it is not possible to achieve perceptible current levels that are below voltage compliance limits when using highly focused stimulation modes (Bierer, 2007). For this reason, a sigma of 0.9 was selected instead of a sigma of 1. Even so, when sigma was set to 0.9, one participant (P08) could not perceive the stimuli at levels that were below the voltage compliance limits of the device. For P08, a sigma of 0.8 was used to measure focused thresholds.

To sweep the stimuli across the electrode array, current was steered between the two active electrodes by varying the steering coefficient, alpha (α). When $\alpha = 0$, all current is delivered through the more apical of the two

active electrodes, and when $\alpha = 1$, all current is steered through the basal active electrode. For Electrodes 3–15, the channel number is the number of the basal active electrode when $\alpha = 1$. An α value of 0 is used to center the current on Electrode 2.

To set the upper limit of stimulation for each threshold sweep procedure, most comfortable listening levels (MCLs) were measured on Channels 2 through 15 in response to the monopolar and focused stimuli. To determine MCL, current level was increased from a subthreshold level of 50 μA until the participant reported a loudness rating of "6" or "most comfortable" on the Advanced Bionics Clinical Loudness Scale. The current level was increased in 2-dB steps until the participant indicated a loudness rating of "4"; thereafter, the level was changed in steps of 0.5 or 0.1 dB. MCLs served as the maximum stimulation level for the threshold sweep procedures.

To measure thresholds in response to both monopolar and focused stimulation, pulse trains were presented starting at 6 dB below MCL and swept across the electrode array. To steer current, alpha was increased from 0 to 1 in step sizes of 0.1. The listener continuously depressed the spacebar on the computer keyboard when he or she could perceive the stimulus and released the spacebar when he or she could not perceive the stimulus. For each stimulus, the participants completed one forward run that swept from Channels 2 to 15 (apical to basal) and one reverse run that swept from Channels 15 to 2 (basal to apical). The weighted average of consecutive current levels along the forward and reverse sweeps were calculated at integer channel numbers to obtain final single-channel threshold estimates (Bierer et al., 2015).

Thresholds were measured on all active electrodes between Electrodes 2 and 15. Note that Subject P02 had two deactivated electrodes in the first implanted ear (Electrodes 7 and 10) and one deactivated electrode in the second implanted ear (Electrode 10). Subject P11 had three deactivated electrodes in the first implanted ear (Electrodes 13–15).

Intracochlear Resistance Measures

Intracochlear resistance was quantified using electrode impedances and EFI. Both measures were included in order to obtain comprehensive and clinically relevant assessments of the impedance environment surrounding the electrode array. Electrode impedances are important in clinical CI programming because they influence the voltage compliance limits of the device and the current levels necessary to elicit auditory percepts. Furthermore, electrode impedances provide insight into the properties of the tissue that are in direct contact with an electrode's surface (Hughes, 2012). Although clinical electrode impedances can provide some insight about the electrode–tissue interface, they do not reflect spatial spread of current throughout the cochlea, and they are influenced by electrode size. EFI provides an estimation of electrical field potentials in addition to individual electrode impedances by recording voltage across the entire electrode array in response to stimulation of a single electrode pair.

Electrode impedances were measured on each active electrode in each ear using the SoundWave clinical impedance measurement software (Advanced Bionics). In Advanced Bionics devices, impedances are tested in monopolar mode. A fixed, low-level current is applied to each electrode, and the corresponding voltage is measured between the active and return electrodes. Impedance, or the resistance to electrical current flow, is calculated via Ohm's law (voltage = current × resistance) using the known current level and voltage output.

EFI stimuli were low-level biphasic, anodic-leading pulses (100-μs duration, either 50 or 100 μA in amplitude) presented in a monopolar stimulation mode at a rate of 16.6 per second. Electrical field potentials were measured by stimulating each intracochlear electrode with 10 consecutive pulses and measuring the voltage across each electrode relative to the monopolar ground (56-kHz sampling rate). Measurements progressed from Electrode 1 to Electrode 16 (apical to basal). The EFI analyses were modeled after those of Vanpoucke, Zarowski, and Peeters (2004), where a detailed explanation of the model can be found.

Briefly, a 16 × 16 impedance matrix was generated from all stimulating/recording combinations and was transformed to solve a lumped parameter resistor network. The solution to the resistor network allowed for electrode-specific estimation of 16 transverse resistances (R_{trans}), 15 longitudinal resistances (R_{long}; Electrodes 2–16), and 16 total resistances (R_{total}). The resistor components of the network, R_{long} and R_{trans}, were estimated using least squares optimization with a localized weighting scheme to improve the EFI profile fit. R_{long} represents the current flow from each electrode along and parallel to the cochlear duct in the basal direction. R_{trans} represents current flow from each electrode to the extracochlear ground. R_{total} is calculated as the peak of the reconstructed EFI profile and estimates the total resistance encountered by the stimulating electrode. R_{long}, R_{trans}, and R_{total} are highly correlated with one another, so only R_{long} was compared across groups in the present analysis. R_{long} was chosen because it has been estimated that the majority of current flows longitudinally along the cochlear duct (Briaire & Frijns, 2000; Jolly, Spelman, & Clopton, 1996; Kumar, Chokshi, & Richter, 2010).

Statistical Analyses

Statistical analyses were performed in R Version 3.3.1 (R Core Team, 2016) using the lmerTest (Kuznetsova, Brockhoff, & Christensen, 2017) and MuMIn (Bartón, 2018) packages. Linear mixed-effects models were used for all electrode-specific analyses to account for repeated measurements within the same subjects. In such cases, "participant" and "ear" were included as random effects in the models. All linear mixed-effects models were fit using restricted maximum likelihood parameter estimates to

minimize small sample estimation bias (McNeish, 2017) and an unstructured covariance matrix.

Results

Table 2 shows descriptive statistics (means and standard deviations) for behavioral thresholds and intracochlear resistance measures, stratified by etiology and electrode site (apical and basal). Table 3 shows results from the linear mixed-effects models predicting behavioral thresholds, electrode impedances, and longitudinal intracochlear resistance. Electrodes 1–8 were considered "apical," and Electrodes 9–16 were considered "basal." Of note, neither duration of deafness, age of implantation, nor vowel identification scores differed between children with EVA and those with DFNB1 (all *p*s > .05).

Single-Channel Auditory Detection Thresholds as a Function of Etiology

The goal of the first analysis was to determine whether single-channel behavioral auditory detection thresholds differ between children with EVA and those with DFNB1. Figure 1 shows average thresholds across the electrode array as a function of etiology, measured in response to both monopolar and focused electrode configurations. Figure 2 shows individual single-channel thresholds as a function of etiology and electrode site. The linear mixed-effects model predicting behavioral thresholds (dependent variable) included etiology, electrode configuration (monopolar or focused), and electrode site (apical or basal) as independent variables. Two interaction terms were also included in the model: (a) etiology by electrode configuration and (b) etiology by electrode site.

Results of the linear mixed-effects model suggested that children with EVA had significantly higher behavioral thresholds than children with DFNB1 ($p = .016$; see Table 3), irrespective of electrode configuration and electrode site. Moreover, there was a significant interaction between etiology and electrode site ($p < .001$; see Table 3). As evidenced in Figures 1 and 2, this finding suggests that differences in thresholds as a function of etiology were larger in the apical region of the cochlea than in the basal region. On average, thresholds were slightly higher (1.06 dB) in the base than in the apex for both groups of subjects ($p = .008$; see Table 3). Across subjects, focused thresholds were higher than monopolar thresholds ($p < .001$; see Table 3). Finally, the interaction between etiology and electrode configuration was not significant, suggesting that differences between monopolar and focused thresholds were similar across etiologies ($p = .146$; see Table 3).

Recall that focused thresholds for Subject P08 were measured using a focusing coefficient of 0.8 because auditory percepts could not be elicited below voltage compliance limits in response to a coefficient of 0.9. Lower focusing coefficients are associated with lower behavioral thresholds than higher coefficients (e.g., Bierer & Faulkner, 2010). Another subject, P15, has a Mid-Scala electrode array, whereas every other subject has a HiFocus 1J electrode array. Different electrode arrays are designed to achieve different positions in the scala tympani (Dhanasingh & Jolly, 2017), which could influence behavioral threshold measurements (DeVries et al., 2016; Long et al., 2014). Sensitivity analyses were conducted to determine whether the same results were obtained when P15 and P08 were excluded from the behavioral threshold model. Removal of neither P08 nor P15 changed the behavioral threshold results. In fact, P08's focused thresholds were among the highest in the sample, despite being measured with a smaller focusing coefficient.

A final exploratory analysis assessed channel-to-channel variability in auditory detection thresholds as a function of etiology. For each ear, channel-to-channel variability was defined as the standard deviation of the signed differences in threshold between each adjacent electrode (as in the study of DiNino et al., 2019). Threshold variability was assessed separately for each electrode configuration. For each electrode configuration, a linear mixed-effects model with a random intercept for "participant" was specified to account for clustering of two ears within the bilaterally implanted participants. Results

Table 2. Descriptive statistics (means and standard deviations) for behavioral thresholds and intracochlear resistance measures, stratified by etiology and cochlear location (apical or basal).

	EVA		DFNB1	
Measurement	**Apical *M* (*SD*)**	**Basal *M* (*SD*)**	**Apical *M* (*SD*)**	**Basal *M* (*SD*)**
Monopolar thresholds (dB re: 1 μA)	35.74 (2.89)	34.72 (3.51)	30.91 (3.56)	31.78 (3.04)
Focused thresholds (dB re: 1 μA)	48.66 (5.19)	45.90 (6.04)	41.81 (4.71)	43.02 (4.80)
Clinical electrode impedances (kΩ)	6.00 (2.67)	6.36 (2.60)	4.40 (1.16)	6.45 (2.89)
Longitudinal resistance (kΩ)	0.89 (0.82)	0.79 (0.93)	0.31 (0.13)	0.66 (0.75)
Transverse resistance (kΩ)	23.02 (15.10)	33.74 (29.16)	16.76 (6.07)	15.12 (6.00)
Total resistance (kΩ)	1.68 (0.79)	1.39 (0.56)	1.24 (0.24)	1.43 (0.69)

Note. For behavioral threshold measurements, data are averaged across Electrodes 2–8 (apical) and Electrodes 9–15 (basal). For intracochlear resistance measures, data are averaged across Electrodes 1–8 (apical; 2–8 for longitudinal resistance) and 9–16 (basal). EVA = enlarged vestibular aqueduct; DFNB1 = connexin-26 genetic mutation.

Table 3. Results from the linear mixed-effects models.

Parameter	Estimate (β)	*SE*	*df*	*t*	*p*
Model predicting behavioral thresholds					
Intercept	41.90	1.28	5.8	32.75	**< .001**
Etiology	6.36	2.07	7.8	3.08	**.016**
Electrode configuration	–11.07	0.37	392.0	–29.97	**< .001**
Electrode site	0.98	0.37	392.2	2.65	**.008**
Etiology × Electrode Site	–2.93	0.64	392.1	–4.58	**< .001**
Etiology × Configuration	–0.93	0.64	392.0	–1.46	.146
Model predicting electrode impedances					
Intercept	4.40	0.79	7.1	5.55	**.001**
Etiology	2.04	1.22	7.8	1.67	.134
Electrode site	2.05	0.28	222.0	7.45	**< .001**
Etiology × Electrode Site	–1.63	0.48	222.1	–3.41	**< .001**
Model predicting longitudinal intracochlear resistance					
Intercept	2.46	0.11	7.3	22.41	**< .001**
Etiology	0.35	0.17	9.5	1.99	.076
Electrode site	0.15	0.08	208.0	2.00	**.047**
Etiology × Electrode Site	–0.48	0.13	208.0	–3.60	**< .001**

Note. The lmer function in *R* calculates *t* tests using Satterthwaite approximations to degrees of freedom (*df*). Statistically significant *p* values are in bold font. Each model included random effects for subject and ear.

suggested that channel-to-channel variability in auditory detection thresholds did not differ as a function of etiology for either monopolar (β = –0.50, *SE* = 0.53), $t(7.98) = -0.94$, $p = .38$, or focused (β = –0.11, *SE* = 0.25), $t(7.57) = -0.45$, $p = .67$, electrode configurations. These results are considered exploratory because, unlike the single-channel threshold data, only one data point was available per ear.

Figure 1. Mean single-channel behavioral thresholds (in dB re: 1 μA) as a function of hearing loss etiology measured in response to monopolar (filled circles) and focused (open circles) electrode configurations. Data from participants with enlarged vestibular aqueduct (EVA) syndrome are represented by green symbols with dashed lines. Data from participants with connexin-26–based mutations (DFNB1) are represented by blue symbols with solid lines. Error bars represent ± 1 standard error.

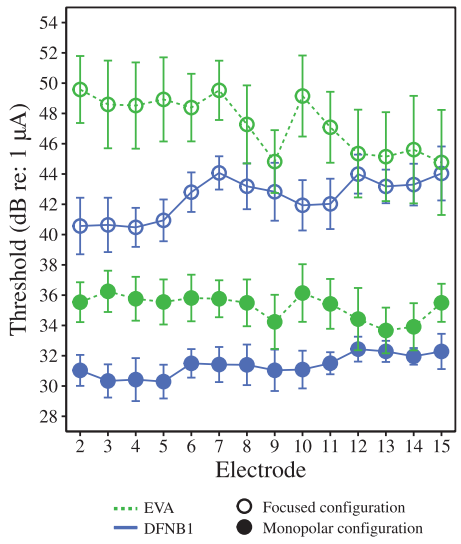

Electrode Impedances as a Function of Etiology

The goal of the second analysis was to determine whether electrode impedances differ between children with EVA and those with DFNB1. Figure 3A shows average impedances across the electrode array as a function of etiology. Figure 3B shows individual single-channel electrode impedances as a function of etiology and electrode site. A linear mixed-effects model predicting electrode impedances (dependent variable) included etiology and electrode site (apical or basal) as independent variables. An interaction between etiology and electrode site was also included in the model.

On average, electrode impedances did not differ as a function of etiology ($p = .134$; see Table 3). However, the interaction between etiology and electrode site was significant, suggesting that children with EVA had significantly higher electrode impedances in the apical region of the cochlea than children with DFNB1 ($p < .001$; see Figure 3 and Table 3). Across subjects, electrode impedances were higher in the base than in the apex ($p < .001$; see Figure 3 and Table 3). Of note, it appears that across-subject variability in electrode impedances is larger for the children with EVA than for the children with DFNB1 (see Figure 3 and Table 3). However, differences in across-subject variability should be interpreted with caution given the small sample size in this study.

An exploratory analysis was performed to assess within-subject variability in electrode impedances across the electrode array as a function of etiology. For each ear, channel-to-channel variability was defined as the standard deviation of the signed differences in electrode impedance between each adjacent electrode. A linear mixed-effects model with a random intercept for "participant" was specified to account for clustering of two ears within the bilaterally implanted participants. Results suggested that channel-to-channel variability in electrode impedances did

Figure 2. (A) Individual single-channel behavioral thresholds (in dB re: 1 μA) measured in response to a monopolar electrode configuration as a function of hearing loss etiology and electrode site (apical or basal). (B) Individual single-channel behavioral thresholds (in dB re: 1 μA) measured in response to a spatially focused electrode configuration as a function of hearing loss etiology and electrode site (apical or basal). Electrodes 2–8 are considered apical, and Electrodes 9–15 are considered basal. Data from participants with enlarged vestibular aqueduct (EVA) are represented by green squares, and data from participants with connexin-26–based mutations (DFNB1) are represented by blue triangles.

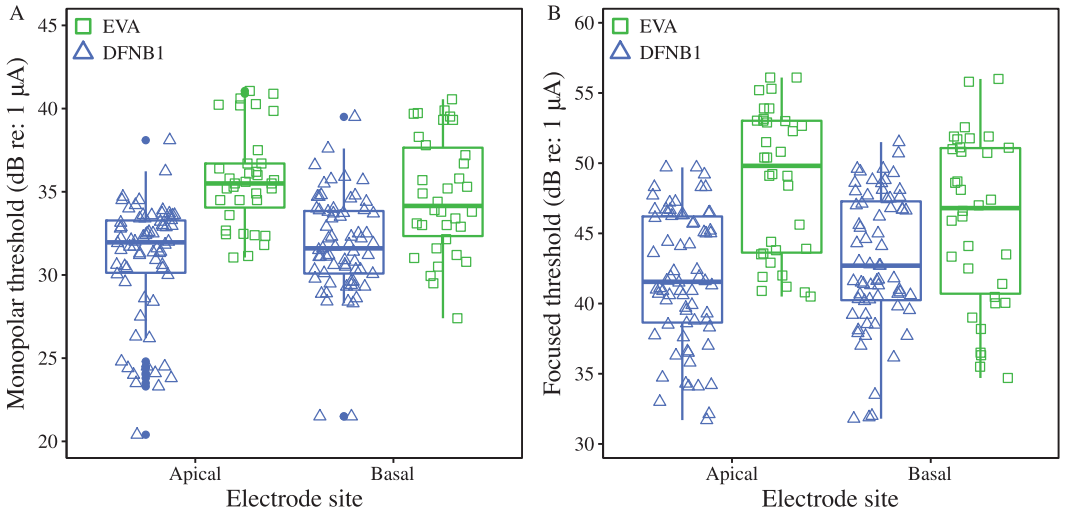

not differ as a function of etiology (β = 0.15, *SE* = 0.30), $t(13.00) = 0.49$, $p = .63$.

Longitudinal Intracochlear Resistance as a Function of Etiology

The goal of the final analysis was to determine whether longitudinal intracochlear resistance, assessed via EFI, differed between children with EVA and children with DFNB1. Figure 4A shows average R_{long} values across the electrode array as a function of etiology. Figure 4B shows individual single-channel R_{long} data as a function of etiology and electrode site. R_{long} values were highly skewed and were consequently log-transformed prior to data analysis in order to reduce skew. A linear mixed-effects model predicting the log-transformed R_{long} values (dependent

Figure 3. (A) Mean electrode impedances (kΩ) as a function of hearing loss etiology. Error bars represent ± 1 standard error. (B) Individual single-channel electrode impedances (kΩ) as a function of electrode site (apical or basal) and hearing loss etiology. Electrodes 1–8 are considered apical, and Electrodes 9–16 are considered basal. Data from participants with enlarged vestibular aqueduct (EVA) are represented by green squares, and data from participants with connexin-26–based mutations (DFNB1) are represented by blue triangles.

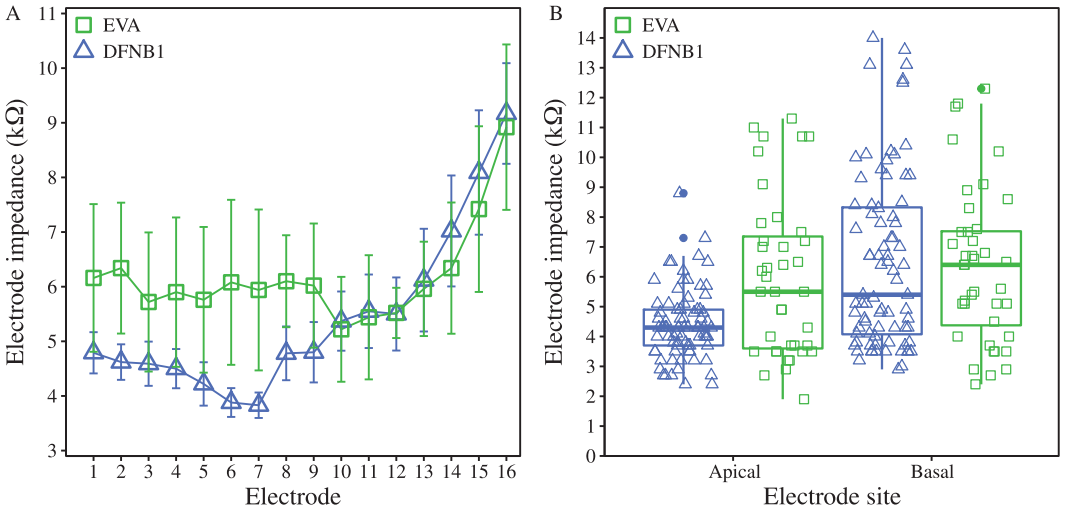

Figure 4. (A) Mean longitudinal intracochlear resistance (kΩ) as a function of hearing loss etiology. Error bars represent ± 1 standard error. (B) Individual single-channel longitudinal intracochlear resistance values (kΩ) as a function of electrode site (apical or basal) and hearing loss etiology. Electrodes 2–8 are considered apical, and Electrodes 9–16 are considered basal. Data from participants with enlarged vestibular aqueduct (EVA) are represented by green squares, and data from participants with connexin-26–based mutations (DFNB1) are represented by blue triangles.

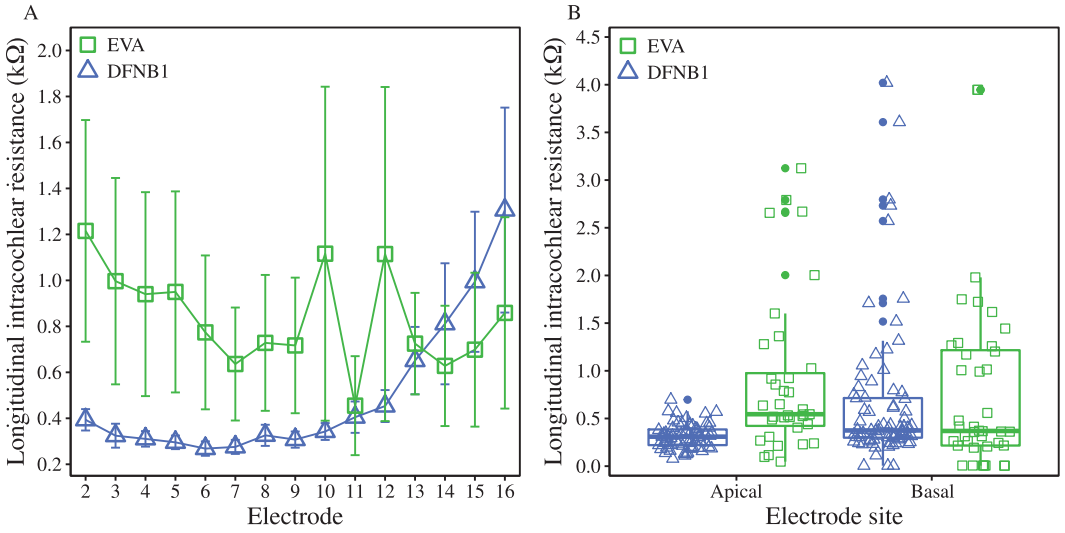

variable) included etiology and electrode site (apical or basal) as independent variables. An interaction between etiology and electrode site was also included in the model.

Results of the EFI analysis were similar to those of the electrode impedance analysis. On average, longitudinal intracochlear resistance did not significantly differ between children with EVA and those with DFNB1 ($p = .076$; see Table 3). However, the interaction between etiology and electrode site was significant, suggesting that longitudinal intracochlear resistance was higher in the apical region for children with EVA than for children with DFNB1 ($p < .001$; see Figure 4 and Table 3). Moreover, across subjects, intracochlear resistance was significantly higher in the base compared to the apex ($p = .047$; see Table 3). Again, it appears that across-subject variability in intracochlear resistance is greater for the children with EVA than for the children with DFNB1 (see Figure 3 and Table 3). However, differences in across-subject variability should be interpreted with caution given the small sample size in this study.

Note that electrode size and spacing differ between the Mid-Scala and HiFocus 1J arrays, which can influence impedance measurements. Once again, a sensitivity analysis was conducted by removing Subject P15 from the electrode impedance and intracochlear resistance analyses. The results did not change when Subject P15's data were excluded.

Finally, an exploratory analysis was performed to assess within-subject variability in longitudinal intracochlear resistance across the electrode array as a function of etiology. For each ear, channel-to-channel variability was defined as the standard deviation of the signed differences in longitudinal intracochlear resistance between each adjacent electrode. A linear mixed-effects model with a random intercept for "participant" was specified to account for clustering of two ears within the bilaterally implanted participants. Results suggested that channel-to-channel variability in longitudinal intracochlear resistance did not differ as a function of etiology ($\beta = 388.7$, $SE = 235.9$), $t(13.00) = 1.65$, $p = .12$.

Relationships Between Resistance and Threshold Measures

Relationships between the single-channel resistance and threshold measures were evaluated. For each analysis, a linear mixed-effects model with "participant" and "ear" as random factors was specified. Across electrodes, longitudinal intracochlear resistance values and electrode impedances were significantly correlated ($\beta = 0.08$, $SE = 0.01$), $t(212.32) = 7.17$, $p < .001$. Electrodes with relatively high electrode impedances also had relatively high EFI-estimated longitudinal intracochlear resistance.

In this sample, longitudinal intracochlear resistance values were not significantly correlated with auditory detection thresholds measured in response to either monopolar ($\beta = 0.57$, $SE = 0.37$), $t(193.33) = 1.56$, $p = .12$, or focused ($\beta = 0.30$, $SE = 0.55$), $t(191.41) = 0.54$, $p = .59$, electrode configurations. Electrode impedances were significantly correlated with monopolar thresholds ($\beta = 0.21$, $SE = 0.09$), $t(198.53) = 2.28$, $p = .02$, but not focused thresholds ($\beta = 0.10$, $SE = 0.14$), $t(196.47) = 0.74$, $p = .46$. In adult CI listeners, previous work shows only modest relationships between auditory detection thresholds and

resistance measures after controlling for computed tomography–estimated electrode position and a behavioral estimate of SGN integrity (Jahn & Arenberg, 2019a).

Discussion

The primary goal of this study was to quantify differences in the ENI related to hearing loss etiology in pediatric CI listeners deafened secondary to EVA and DFNB1. The ENI was assessed using single-channel auditory detection thresholds, electrode impedances, and EFI. Results demonstrated that children with EVA had higher single-channel auditory detection thresholds than children with DFNB1. Children with EVA also had higher cochlear resistivity in the apical region of the cochlea than children with DFNB1. Taken together, these results suggest that the ENI differs as a function of hearing loss etiology in pediatric CI listeners.

Higher Auditory Detection Thresholds in Children With EVA Than in Children With DFNB1

In this study, we observed higher single-channel auditory detection thresholds in pediatric CI listeners with EVA than in listeners with DFNB1, irrespective of the electrode configuration (monopolar or spatially focused). Previous research suggests that electrode placement relative to the modiolus is one of the strongest predictors of single-channel behavioral threshold levels (DeVries et al., 2016; Long et al., 2014). Furthermore, van der Marel et al. (2014) demonstrated that the size of the cochlea influences the placement of the electrodes, wherein increases in cochlear diameter are associated with increases in the physical distance between CI electrodes and the modiolus.

It is possible that the placement of the electrode array relative to the modiolus could be systematically altered in patients with EVA, who frequently have some degree of cochlear dysplasia (Davidson et al., 1999). Davidson et al. (1999) reported that individuals with EVA and mild cochlear dysmorphia tended to have broad contours in the apical region of the cochlea and an absence of the notch between the apical and lateral middle turns. Those with severely dysmorphic inner ears also demonstrated a loss of internal cochlear architecture (Davidson et al., 1999). Such malformations would likely result in electrode array placement farther from the modiolus in patients with EVA compared to patients with DFNB1, who tend to have normal cochlear anatomy. If children with EVA tend to have poor electrode placement, they may be good candidates for perimodiolar electrode arrays that attempt to position the electrodes relatively close to the modiolus. Imaging studies that systematically evaluate electrode array placement as a function of etiology are warranted.

In addition to electrode position, the integrity of the SGNs is believed to influence single-channel threshold levels (DeVries et al., 2016; George, Wise, Fallow, & Shepherd, 2015; George, Wise, Shivdasani, Sheperd, & Fallon, 2014; Goldwyn et al., 2010; Jahn & Arenberg, 2019a, 2019b). Computational modeling evidence suggests that SGN loss can lead to increased behavioral thresholds and faster growth of neural recruitment with increasing stimulation levels (Goldwyn et al. 2010). In humans, channels with relatively high behavioral thresholds also exhibit relatively small evoked potential amplitudes (DeVries et al., 2016), which are associated with reduced SGN density in animal models (Ramekers et al., 2014). Thus, electrodes located near cochlear regions with relatively poor neural health are expected to have relatively high auditory detection thresholds.

Importantly, previous work indicates that almost all patients with EVA have some degree of modiolar deficiency (Davidson et al., 1999; Lemmerling et al., 1997). Because the SGNs are housed within the bony modiolus, it is plausible that pervasive modiolar deficiencies in individuals with EVA could lead to reduced integrity or density of viable SGNs relative to normal. Limited histopathological evidence in a patient with EVA and incomplete partition type II cochlear anomaly demonstrated abnormally formed neural structures in the apex, but enough viable SGNs in the basal turn to achieve adequate electrical stimulation in the base (Leung, Quesnel, Juliano, & Curtin, 2016). In contrast, histopathological evidence in a patient with Cx26-based deafness showed normal populations of SGNs throughout the cochlea (Jun et al., 2000). Recent electrophysiological data demonstrate that children with Cx26 mutations may have better auditory nerve function than children with concurrent Mondini malformation and EVA (Luo et al., 2019). Overall, available evidence suggests that higher behavioral thresholds in children with EVA than in children with DFNB1 could plausibly be explained by a less robust population of functional SGNs, a larger physical distance between the electrodes and the modiolus, or a combination of the two factors. These differences appear to be most pronounced in the apex, consistent with available histopathological data in patients with EVA.

Higher Apical Intracochlear Resistance in Children With EVA Than in Children With DFNB1

In this study, electrode impedances and longitudinal intracochlear resistance values were higher in the apical region of the cochlea in children with EVA than in children with DFNB1. Cochlear resistivity did not differ between groups in the basal region of the cochlea or when averaged across all electrodes. One study by Powell and Birman (2015) also showed that average electrode impedances did not differ between children with EVA and those with other hearing loss etiologies. Our results demonstrate the importance of considering electrode location and single-channel data when evaluating the ENI in children.

Though little is understood about intracochlear bone and fibrous tissue growth in children with EVA, recall that even mild EVA-associated cochlear malformations appear to be most pronounced in the apex (Davidson et al., 1999; Leung et al., 2016). It is possible that cochlear and modiolar

malformations differentially influence the electrode–tissue interface in the apex compared to the base in individuals with EVA. Moreover, we noted particularly high variability in cochlear resistivity measurements across ears and electrode sites in the children with EVA. This could reflect within- and across-ear variation in cochlear and modiolar morpohology in patients with EVA. The present results support available histological and electrophysiological data and indicate that further investigation into differences in cochlear resistivity as a function of hearing loss etiology is warranted.

Clinical Implications and Future Directions

The results of this study demonstrate that multiple factors influencing the quality of the ENI may differ between pediatric CI listeners with EVA and those with DFNB1. It should be noted that, despite potential differences in the ENI, both children with EVA and those with DFNB1 receive good speech perception benefit from currently available clinical CI interventions (e.g., Ahadizadeh et al., 2017; Aimoni et al., 2017; Manzoor et al., 2016; Papsin, 2005; Wu et al., 2015; Yan et al., 2013). However, given the persistent variability in outcomes across all pediatric CI listeners, it is imperative to determine methods for optimizing clinical interventions based on a patient's unique demographic characteristics and auditory goals. The results of this study suggest that differences in the ENI related to hearing loss etiology may help to identify optimal CI programming parameters for children with divergent hearing histories.

The present results suggest that children with EVA may have a larger physical distance between the electrodes and the modiolus and/or reduced SGN integrity relative to children with DFNB1. A large-scale study that estimates electrode position using computed tomography imaging in conjunction with electrode-specific evoked potential estimates that are correlated with neural health in animal models may help elucidate the origin of between-group threshold differences. If children with DFNB1 have robust populations of functional SGNs, they may be good candidates for CI programming strategies that employ current focusing to more selectively stimulate local auditory nerve fibers and reduce channel interaction. There is evidence that reducing channel interaction may be particularly beneficial to speech perception outcomes of children with CIs (Jahn, DiNino, & Arenberg, 2019).

In contrast, the results of this study suggest that high degrees of current focusing may not be optimal for listeners with EVA, as it can be difficult to achieve comfortably loud stimulus levels in CI listeners that have high auditory detection thresholds and/or high electrode impedances. In fact, recall that Subject P08 in this study could not detect stimuli at levels below the voltage compliance limits of the device with a high current focusing coefficient. An inability to reach comfortably loud stimulation levels could unnecessarily restrict the electrical dynamic range and limit loudness growth, potentially negating positive perceptual effects of extreme current focusing.

Instead, listeners with EVA may be more likely to benefit from programming changes that reduce the current levels necessary to optimize dynamic range while remaining below the voltage compliance limits of the device. For instance, it is possible that listeners with EVA could benefit from low-to-moderate degrees of current focusing (i.e., focusing coefficient < 0.9), relatively wide stimulation pulse widths, or relatively long interphase gaps. In fact, there is evidence that individuals with malformed cochleae tend to require wider pulse widths than listeners with normal cochlear anatomy (Coelho & Roland, 2012; Incerti et al., 2018; Papsin, 2005). Knowledge that a CI listener with EVA is likely to require different stimulation parameters may be particularly important for clinicians working with infants and young children who cannot provide reliable feedback or behavioral information.

It is acknowledged that this preliminary study was conducted with a small sample of CI listeners. This investigation should be replicated in a larger group of children, with particular emphasis on measurements that can distinguish between electrode placement and the integrity of the auditory neurons. Future investigations will examine common clinical programming parameters in a large sample of pediatric CI listeners and will determine whether current focusing is beneficial for children with a variety of hearing loss etiologies.

Acknowledgments

This work was supported by National Institute on Deafness and Other Communication Disorders Grants R01 DC012142 (awarded to J. G. A.) and T32 DC005361 (awarded to K. N. J.; PI: Perkel). The authors thank Susan Norton, David Horn, and Wendy Parkinson for assistance with participant recruitment. The authors also thank their devoted participants for their time.

References

Ahadizadeh, E., Ascha, M., Manzoor, N., Gupta, A., Semaan, M., Megerian, C., & Otteson, T. (2017). Hearing loss in enlarged vestibular aqueduct and incomplete partition type II. *American Journal of Otolaryngology, 38*(6), 692–697. https://doi.org/10.1016/j.amjoto.2017.06.010

Aimoni, C., Ciorba, A., Cerritelli, L., Ceruti, S., Skarżyński, P. H., & Hatzopoulos, S. (2017). Enlarged vestibular aqueduct: Audiological and genetical features in children and adolescents. *International Journal of Pediatric Otorhinolaryngology, 101,* 254–258. https://doi.org/10.1016/j.ijporl.2017.07.042

Bartón, K. (2018). MuMIn: Multi-Modal Inference (R package Version 1.43.6). Retrieved from https://CRAN.R-project.org/package=MuMIn

Berrettini, S., Forli, F., Bogazzi, F., Neri, E., Salvatori, L., Casani, A. P., & Franceschini, S. S. (2005). Large vestibular aqueduct syndrome: Audiological, radiological, clinical, and genetic features. *American Journal of Otolaryngology, 26*(6), 363–371. https://doi.org/10.1016/j.amjoto.2005.02.013

Bierer, J. A. (2007). Threshold and channel interaction in cochlear implant users: Evaluation of the tripolar electrode configuration. *The Journal of the Acoustical Society of America, 121*(3), 1642–1653. https://doi.org/10.1121/1.2436712

Bierer, J. A., Bierer, S. M., Kreft, H. A., & Oxenham, A. J. (2015). A fast method for measuring psychophysical thresholds across the cochlear implant array. *Trends in Hearing, 19,* 1–12. https://doi.org/10.1177/2331216515569792

Bierer, J. A., & Faulkner, K. F. (2010). Identifying cochlear implant channels with poor electrode–neuron interface: Partial tripolar, single-channel thresholds and psychophysical tuning curves. *Ear and Hearing, 31*(2), 247–258. https://doi.org/10.1097/AUD.0b013e3181c7daf4

Briaire, J. J., & Frijns, J. H. (2000). Field patterns in a 3D tapered spiral model of the electrically stimulated cochlea. *Hearing Research, 148*(1–2), 18–30.

Coelho, D. H., & Roland, J. T., Jr. (2012). Implanting obstructed and malformed cochleae. *Otolaryngologic Clinics of North America, 45*(1), 91–110. https://doi.org/10.1016/j.otc.2011.08.019

Cohn, E. S., Kelley, P. M., Fowler, T. W., Gorga, M. P., Lefkowitz, D. M., Keuhn, H. J., . . . Kimberling, W. J. (1999). Clinical studies of families with hearing loss attributable to mutations in the connexin 26 gene (GJB2/DFNB1). *Pediatrics, 103*(3), 546–550. https://doi.org/10.1542/peds.103.3.546

Dahl, H. H., Saunders, K., Kelly, T. M., Osborn, A. H., Wilcox, S., Cone-Wesson, B., . . . Mutton, P. (2001). Prevalence and nature of connexin 26 mutations in children with non-syndromic deafness. *The Medical Journal of Australia, 175*(4), 191–194.

Davidson, H. C., Harnsberger, H. R., Lemmerling, M. M., Mancuso, A. A., White, D. K., Tong, K. A., . . . Shelton, C. (1999). MR evaluation of vestibulocochlear anomalies associated with large endolymphatic duct and sac. *American Journal of Neuroradiology, 20*(8), 1435–1441.

Del Castillo, F. J., & Del Castillo, I. (2017). DFNB1 non-syndromic hearing impairment: Diversity of mutations and associated phenotypes. *Frontiers in Molecular Neuroscience, 10,* 428. https://doi.org/10.3389/fnmol.2017.00428

DeVries, L., Scheperle, R., & Bierer, J. A. (2016). Assessing the electrode–neuron interface with the electrically evoked compound action potential, electrode position, and behavioral thresholds. *Journal of the Association for Research in Otolaryngology, 17*(3), 237–252. https://doi.org/10.1007/s10162-016-0557-9

Dhanasingh, A., & Jolly, C. (2017). An overview of cochlear implant electrode array designs. *Hearing Research, 356,* 93–103. https://doi.org/10.1016/j.heares.2017.10.005

DiNino, M., & Arenberg, J. G. (2018). Age-related performance on vowel identification and the spectral-temporally modulated ripple test in children with normal hearing and with cochlear implants. *Trends in Hearing, 22,* 1–20. https://doi.org/10.1177/2331216518770959

DiNino, M., O'Brien, G., Bierer, S. M., Jahn, K. N., & Arenberg, J. G. (2019). The estimated electrode-neuron interface in cochlear implant listeners is different for early-implanted children and late-implanted adults. *Journal of the Association for Research in Otolaryngology, 20*(3), 291–303. https://doi.org/10.1007/s10162-019-00716-4

Durisin, M., Büchner, A., Lesinski-Schiedat, A., Bartling, S., Warnecke, A., & Lenarz, T. (2015). Cochlear implantation in children with bacterial meningitic deafness: The influence of the degree of ossification and obliteration on impedance and charge of the implant. *Cochlear Implants International, 16*(3), 147–158. https://doi.org/10.1179/1754762814Y.0000000094

Eisenman, D. J., Ashbaugh, C., Zwolan, T. A., Arts, H. A., & Telian, S. A. (2001). Implantation of the malformed cochlea. *Otology & Neurotology, 22*(6), 834–841. https://doi.org/10.1097/00129492-200111000-00020

Eshraghi, A. A., Telischi, F. F., Hodges, A. V., Odabasi, O., & Balkany, T. J. (2004). Changes in programming over time in postmeningitis cochlear implant users. *Otolaryngology—Head & Neck Surgery, 131*(6), 885–889. https://doi.org/10.1016/j.otohns.2004.05.019

George, S. S., Wise, A. K., Fallon, J. B., & Shepherd, R. K. (2015). Evaluation of focused multipolar stimulation for cochlear implants in long-term deafened cats. *Journal of Neural Engineering, 12*(6), 1–15. https://doi.org/10.1088/1741-2560/12/3/036003

George, S. S., Wise, A. K., Shivdasani, M. N., Shepherd, R. K., & Fallon, J. B. (2014). Evaluation of focused multipolar stimulation for cochlear implants in acutely deafened cats. *Journal of Neural Engineering, 11*(6), 1–13. https://doi.org/10.1088/1741-2560/11/6/065003

Goldwyn, J. H., Bierer, S. M., & Bierer, J. A. (2010). Modeling the electrode–neuron interface of cochlear implants: Effects of neural survival, electrode placement, and the partial tripolar configuration. *Hearing Research, 268*(1–2), 93–104. https://doi.org/10.1016/j.heares.2010.05.005

He, S., Shahsavarani, B. S., McFayden, T. C., Wang, H., Gill, K. E., Xu, L., Chao, X., . . . He, N. (2018). Responsiveness of the electrically stimulated cochlear nerve in children with cochlear nerve deficiency. *Ear and Hearing, 39*(2), 238–250. https://doi.org/10.1097/AUD.0000000000000467

Huber, M., & Kipman, U. (2012). Cognitive skills and academic achievement of deaf children with cochlear implants. *Otolaryngology—Head & Neck Surgery, 147*(4), 763–772. https://doi.org/10.1177/0194599812448352

Hughes, M. L. (2012). *Objective measures in cochlear implants*. San Diego, CA: Plural. Retrieved from http://ebookcentral.proquest.com

Incerti, P. V., Ching, T. Y. C., Hou, S., Van Buynder, P., Flynn, C., & Cowan, R. (2018). Programming characteristics of cochlear implants in children: Effects of aetiology and age at implantation. *International Journal of Audiology, 57*(Suppl. 2), S27–S40. https://doi.org/10.1080/14992027.2017.1370139

Ito, T., Li, X., Kurima, K., Choi, B. Y., Wangemann, P., & Griffith, A. J. (2014). Slc26a4-insufficiency causes fluctuating hearing loss and stria vascularis dysfunction. *Neurobiology of Disease, 66,* 53–65. https://doi.org/10.1016/j.nbd.2014.02.002

Jahn, K. N., & Arenberg, J. G. (2019a). Evaluating psychophysical polarity sensitivity as an indirect estimate of neural status in cochlear implant listeners. *Journal of the Association for Research in Otolaryngology, 20*(4), 415–430. https://doi.org/10.1007/s10162-019-00718-2

Jahn, K. N., & Arenberg, J. G. (2019b). Polarity sensitivity in pediatric and adult cochlear implant listeners. *Trends in Hearing, 23,* 1–22. https://doi.org/10.1177/2331216519862987

Jahn, K. N., DiNino, M., & Arenberg, J. G. (2019). Reducing simulated channel interaction reveals differences in phoneme identification between children and adults with normal hearing. *Ear and Hearing, 40*(2), 295–311. https://doi.org/10.1097/AUD.0000000000000615

Jolly, C. N., Spelman, F. A., & Clopton, B. M. (1996). Quadrupolar stimulation for cochlear prostheses: Modeling and experimental data. *IEEE Transactions on Biomedical Engineering, 43*(8), 857–865. https://doi.org/10.1109/10.508549

Jun, A. I., McGuirt, W. T., Hinojosa, R., Green, G. E., Fischel-Ghodsian, N., & Smith, R. J. (2000). Temporal bone histopathology in connexin 26-related hearing loss. *The Laryngoscope, 110*(2, Pt. 1), 269–275. https://doi.org/10.1097/00005537-200002010-00016

Kemperman, M. H., Hoefsloot, L. H., & Cremers, C. W. R. J. (2002). Hearing loss and connexin 26. *Journal of the Royal Society of Medicine, 95*(4), 171–177. https://doi.org/10.1258/jrsm.95.4.171

Kumar, G., Chokshi, M., & Richter, C. P. (2010). Electrical impedance measurements of cochlear structures using the four-electrode reflection-coefficient technique. *Hearing Research, 259*(1–2), 86–94. https://doi.org/10.1016/j.heares.2009.10.010

Kuznetsova, A., Brockhoff, P. B., & Christensen, R. H. B. (2017). lmertest package: Tests in linear mixed effects models. *Journal of Statistical Software, 82*(13). https://doi.org/10.18637/jss.v082.i13

Lemmerling, M. M., Mancuso, A. A., Antonelli, P. J., & Kubilis, P. S. (1997). Normal modiolus: CT appearance in patients with a large vestibular aqueduct. *Radiology, 204*(1), 213–219. https://doi.org/10.1148/radiology.204.1.9205250

Leung, K. J., Quesnel, A. M., Juliano, A. F., & Curtin, H. D. (2016). Correlation of CT, MR, and histopathology in incomplete partition-II cochlear anomaly. *Otology & Neurotology, 37*(5), 434–437. https://doi.org/10.1097/MAO.0000000000001027

Long, C. J., Holden, T. A., McClelland, G. H., Parkinson, W. S., Shelton, C., Kelsall, D. C., & Smith, Z. M. (2014). Examining the electro-neural interface of cochlear implant users using psychophysics, CT scans, and speech understanding. *Journal of the Association for Research in Otolaryngology, 15*(2), 293–304. https://doi.org/10.1007/s10162-013-0437-5

Luo, J., Xu, L., Chao, X., Wang, R., Pellittieri, A., Bai, X., Fan, Z., … He, S. (2019). The effects of GJB2 or SLC26A4 gene mutations on neural response of the electrically stimulated auditory nerve in children. *Ear and Hearing*. Advance online publication. https://doi.org/10.1097/AUD.0000000000000744

Manzoor, N. F., Wick, C. C., Wahba, M., Gupta, A., Piper, R., Murray, G. S., … Semaan, M. T. (2016). Bilateral sequential cochlear implantation in patients with enlarged vestibular aqueduct (EVA) syndrome. *Otology & Neurotology, 37*(2), e96–e103. https://doi.org/10.1097/MAO.0000000000000925

McNeish, D. (2017). Small sample methods for multilevel modeling: A colloquial elucidation of REML and the Kenward-Roger correction. *Multivariate Behavioral Research, 52*(5), 661–670. https://doi.org/10.1080/00273171.2017.1344538

National Institute on Deafness and Other Communication Disorders. (2017). *Enlarged vestibular aqueducts and childhood hearing loss.* Retrieved from https://www.nidcd.nih.gov/health/enlarged-vestibular-aqueducts-and-childhood-hearing-loss

Nelson, D. A., Donaldson, G. S., & Kreft, H. (2008). Forward-masked spatial tuning curves in cochlear implant users. *The Journal of the Acoustical Society of America, 123*(3), 1522–1543. https://doi.org/10.1121/1.2836786

Niparko, J. K., Tobey, E. A., Thal, D. J., Eisenberg, L. S., Wang, N. Y., Quittner, A. L., … CDaCI Investigative Team. (2010). Spoken language development in children following cochlear implantation. *Journal of the American Medical Association, 303*(15), 1498–1506. https://doi.org/10.1001/jama.2010.451

Padilla, M., & Landsberger, D. M. (2016). Reduction in spread of excitation from current focusing at multiple cochlear locations in cochlear implant users. *Hearing Research, 333,* 98–107. https://doi.org/10.1016/j.heares.2016.01.002

Papsin, B. C. (2005). Cochlear implantation in children with anomalous cochleovestibular anatomy. *The Laryngoscope, 115*(1, Pt. 2, Suppl. 106), 1–26. https://doi.org/10.1097/00005537-200501001-00001

Powell, H. R., & Birman, C. S. (2015). Large vestibular aqueduct syndrome: Impedance changes over time with different cochlear implant electrode arrays. *Cochlear Implants International, 16*(6), 326–330. https://doi.org/10.1179/1754762815Y.0000000013

R Core Team. (2016). R: A language and environment for statistical computing. *R Foundation for Statistical Computing, Vienna, Austria, Vienna, Austria*. Retrieved from https://www.R-project.org/

Ramekers, D., Versnel, H., Strahl, S. B., Smeets, E. M., Klis, S. F., & Grolman, W. (2014). Auditory-nerve responses to varied inter-phase gap and phase duration of the electric pulse stimulus as predictors for neuronal degeneration. *Journal of the Association for Research in Otolaryngology, 15*(2), 187–202. https://doi.org/10.1007/s10162-013-0440-x

Sarant, J. Z., Harris, D. C., & Bennet, L. A. (2015). Academic outcomes for school-aged children with severe–profound hearing loss and early unilateral and bilateral cochlear implants. *Journal of Speech, Language, and Hearing Research, 58*(3), 1017–1032. https://doi.org/10.1044/2015_JSLHR-H-14-0075

Sek, A., Alcántara, J., Moore, B. C., Kluk, K., & Wicher, A. (2005). Development of a fast method for determining psychophysical tuning curves. *International Journal of Audiology, 44*(7), 408–420. https://doi.org/10.1121/1.4808787

Spelman, F. A., Clopton, B. M., & Pfingst, B. E. (1982). Tissue impedance and current flow in the implanted ear. Implications for the cochlear prosthesis. *Annals of Otology, Rhinology & Laryngology, 98,* 3–8.

van der Marel, K. S., Briaire, J. J., Wolterbeek, R., Snel-Bongers, J., Verbist, B. M., & Frijns, J. H. (2014). Diversity in cochlear morphology and its influence on cochlear implant electrode position. *Ear and Hearing, 35,* e9–e20. https://doi.org/10.1097/01.aud.0000436256.06395.63

Vanpoucke, F. J., Zarowski, A. J., & Peeters, S. A. (2004). Identification of the impedance model of an implanted cochlear prosthesis from intracochlear potential measurements. *IEEE Transactions on Bio-medical Engineering, 51*(12), 2174–2183. https://doi.org/10.1109/tbme.2004.836518

Vijayasekaran, S., Halsted, M. J., Boston, M., Meinzen-Derr, J., Bardo, D. M., Greinwald, J., & Benton, C. (2007). When is the vestibular aqueduct enlarged? A statistical analysis of the normative distribution of vestibular aqueduct size. *American Journal of Neuroradiology, 28*(6), 1133–1138. https://doi.org/10.3174/ajnr.A0495

Wu, C.-M., Ko, H.-C., Tsou, Y.-T., Lin, Y.-H., Lin, J.-L., Chen, C.-K., … Wu, C.-C. (2015). Long-term cochlear implant outcomes in children with GJB2 and SLC26A4 mutations. *PLOS ONE, 10*(9), e0138575. https://doi.org/10.1371/journal.pone.0138575

Yan, Y., Li, Y., Yang, T., Huang, Q., & Wu, H. (2013). The effect of GJB2 and SLC26A4 gene mutations on rehabilitative outcomes in pediatric cochlear implant patients. *European Archives of Oto-Rhino-Laryngology, 270*(11), 2865–2870. https://doi.org/10.1007/s00405-012-2330-y

Zhu, Z., Tang, Q., Zeng, F. G., Guan, T., & Ye, D. (2012). Cochlear-implant spatial selectivity with monopolar, bipolar and tripolar stimulation. *Hearing Research, 283*(1–2), 45–58. https://doi.org/10.1016/j.heares.2011.11.005